Arabian Journal of Geosciences (2021) 14: 1262
https://doi.org/10.1007/s12517-021-07584-4

ORIGINAL PAPER

Spatio-temporal evolution and future scenario prediction of karst rocky desertification based on CA–Markov model

Fei Chen[1,2,3] · Shijie Wang[2,3] · Xiaoyong Bai[1,2,3] · Fang Liu[1] · Yichao Tian[2,3] · Guangjie Luo[4] · Qin Li[2,3] · Jingfeng Wang[1,2,3] · Luhua Wu[2,3] · Yue Cao[2,3] · Huiwen Li[2,3] · Yuanhong Deng[2,3] · Chaojun Li[2,3] · Yujie Yang[2,3] · Shiqi Tian[2,3] · Qian Lu[1,2,3] · Zheyin Hu[2,3] · Huipeng Xi[2,3]

Received: 18 October 2018 / Accepted: 30 January 2021 / Published online: 26 June 2021

Abstract
Although the cellular automata (CA) model has been extensively applied in the simulation of ground cover changes, but it is rarely applied in the simulation of the driving forces of karst rock desertification (KRD). KRD has become one of the most serious ecological disasters in southwest China. Thus, it is necessary to accurately identify the driving factors affecting the occurrence and development of KRD. Accurately predicting the future development trend of KRD has great significance for quantitative evaluation of ecological environment governance and restoration in karst areas. We used the actual interpretation of KRD data in 2011 and 2016, based on the geographical detector to select the driving factors for the occurrence and development of KRD, and used the CA model to simulate the spatial and temporal changes of KRD. Results show that (1) the kappa verification accuracy for all types of KRD was above 0.5 when the CA model was used for the simulation of the spatial distribution of KRD and thus the theoretical requirements for accurate identification of the distribution of KRD were met. (2) Driving factors can be accurately screened by using the geodetector model to analyze the driving factors of KRD. The strengths of the factors follow the order lithology (0.35) > population density (0.30) > slope (0.21) > soil erosion (0.16) > altitude (0.05). (3)The combination of geodetector and the CA–Markov model results in the accurate prediction of the evolution of KRD and reduction in the arbitrariness of artificial subjective selection factors and the possibility of misjudgement. (4) From 2011 to 2021, the total area of KRD in the study area decreased at a rate of 29.96 $km^2 \cdot a^{-1}$, and KRD land indicated an overall trend of improvement. (5) Under the trend of overall improvement of KRD, some areas remain in which KRD increased and worsened. In the process of governance and protection, the impact of such deterioration on ecological environment must be considered.

Keywords Karst rocky desertification · Geodetector · Cellular automata · Markov · Spatial evolution

Introduction

South China Karst represents the most typical tropical–subtropical karst contiguous area in the world (Wang et al. 2003). Karst rocky desertification (KRD) is widely distributed and has become the most serious ecological disaster (Wang et al. 2004; Wang 2002; Bai et al. 2013; Xiong et al. 2009), which seriously affecting the living environment and standards of the local people, causing a series of social problems (Yuan 2008; Li et al. 2006).

In view of the importance and harmfulness of KRD, many researchers studied the temporal and spatial evolutions of KRD. Yang et al. based on the rock bare rate and vegetation cover (Yang et al. 2011). Zuo et al. used the visual interpretation method by the nudity of rock, and the spatial and temporal evolution of KRD in the karst area of northern Guangxi was studied (Zuo

Responsible Editor: Biswajeet Pradhan

✉ Xiaoyong Bai
baixiaoyong@vip.skleg.cn

1 College of Resources and Environmental Engineering, Guizhou University, Guiyang 550025, China

2 State Key Laboratory of Environmental Geochemistry, Institute of Geochemistry, Chinese Academy of Sciences, 99 Lincheng West Road, Guiyang 550081, Guizhou Province, China

3 Puding Karst Ecosystem Observation and Research Station, Chinese Academy of Sciences, Puding 562100, Guizhou Province, China

4 Guizhou Provincial Key Laboratory of Geographic State Monitoring of Watershed, Guizhou Education University, Guiyang 550018, Guizhou Province, China

et al. 2014). However, most of the research periods selected in previous studies were mostly before 2015. Thus, it is difficult to evaluate the effect of the rocky desertification control project implemented in the past 5 years. Previous studies have significantly contributed to the historical process of the evolution of KRD, but in the quantitative level owing to limited research data and computational ability. The cellular automata (CA) was proposed by Von Neumann J. and Stanislaw M. Ulam in the late 1940s for the simulation of the future scenarios of surface cover-up (Neumann 1996). For instance, many interconnected turing machines may be placed in a grid. Wolfram proved that the CA model can simulate complex natural phenomena and establish the basis of the CA theory (Wolfram 1984; Wolfram 2002). In previous studies, CA are widely employed in land use change (Lambin and Geist 2006; Geist 2006; Wang and Li 2011), urban expansion simulation (Arsanjani et al. 2013; Sun et al. 2012; Long et al. 2009; Qiu and Chen 2008), fire simulation (Berjak and Hearne 2002; Perry 1998; Quartieri et al. 2010; Yassemi et al. 2008), ecology (Muci et al. 2012; Rasmussen and Hamilton 2012; Perez and Dragicevic 2012; Yang et al. 2009) and traffic flow simulation (Han and Ko 2012; Jin and White 2012; Lárraga and Alvarez-Icaza 2010), and other fields. The above research indicates that the application of cellular automaton is mainly applied in the field of land use simulation, but the research in the field of KRD simulation remains scarce.

In this study, we used the remote sensing and geographic information technology to interpretation of KRD, and based on geodetector screen the main driving factors, and predict the spatial pattern and evolutionary trajectory of KRD in 2016 and 2021 by using CA. We use two methods to verify the prediction results accurately, and the results show that all pass the test. The results of this study will serve as bases for government decision-makers and environmental managers for the mitigation of the negative impact of KRD disasters on society and economy.

Materials and methods

Study area

The Yinjiang County is located in Tongren, Guizhou Province, China, the northeast Guizhou plateau. Yinjiang rivers of Wujiang river water system in the Yangtze river basin watershed areas (Fig. 1). The geographical position is 108°17′ to 108°48′E, 26°35′ to 28°28′N. The main peak of the Wuling Mountains Fanjingshan is located in the east of Yinjiang County, forming a high east and west low, southeast to northwest tilt topography, the relative elevation of 2000 m, with average elevation of 2493.8 m.

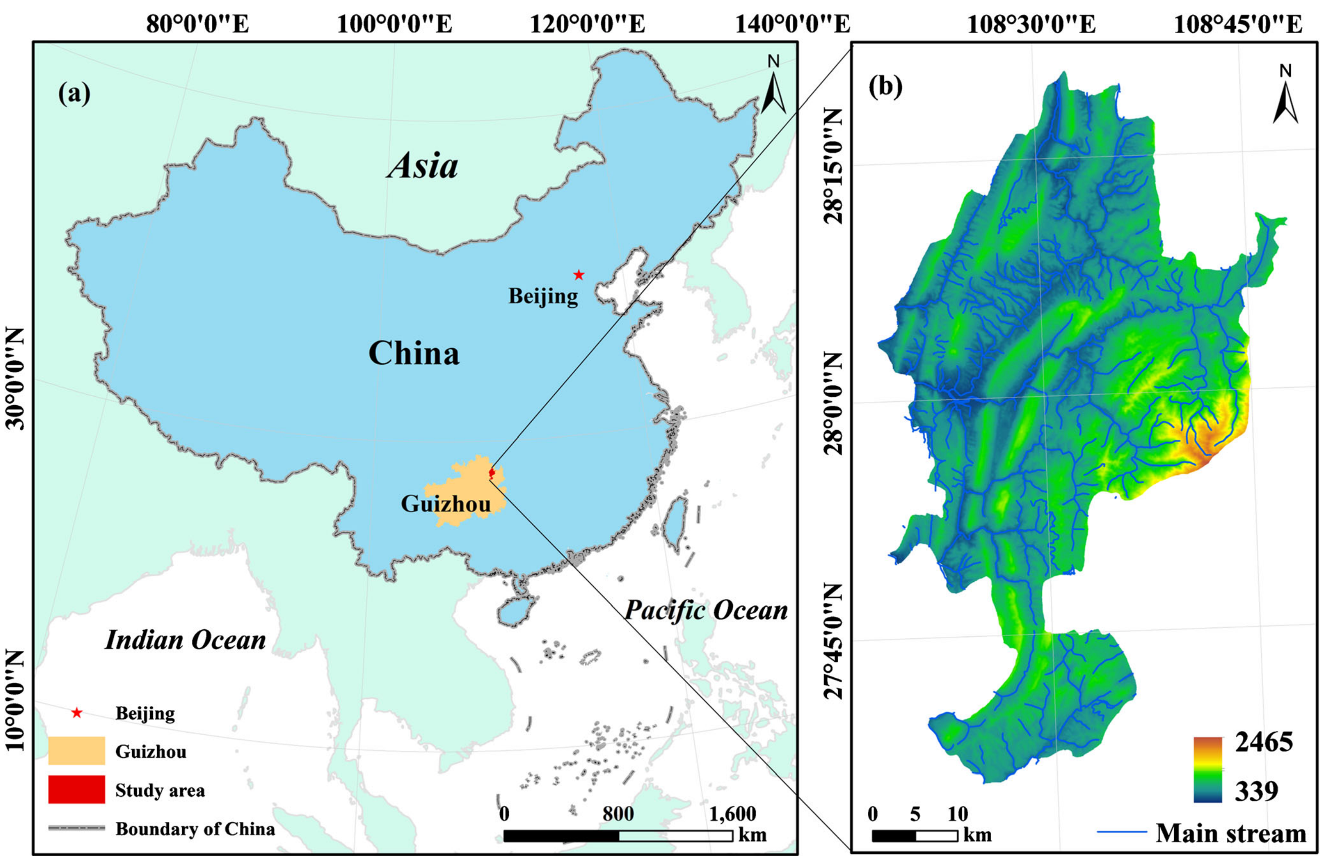

Fig. 1 The location of study area. (We make this map by ArcGIS9.3 (http://www.esri.com/arcgis/about-arcgis))

The main tectonic line in Yinjiang County is Northeast-Southeast distribution and well-developed karst trough is developed in the country. It is a typical area of KRD research. The main lithology in the territory is mainly carbonate rock, accounting for 51.74% of the total carbonate rock, mainly limestone clastic rocks and interbedded layers. The climate is subtropical humid monsoon climate, with an average annual temperature of 16.8 °C and an annual rainfall of about 1100 mm. The slope of the study area is mainly in the range of 5–25°, and soil erosion is dominated by mild erosion. The total population of the study area is about 437,600, but in recent years, the number of go-outside labors has increased, and the resident population is 221,000.

Data and preprocessed

KRD interpretation data sources from Landsat TM 2011 and Landsat OLI 2016 remote sensing images with a resolution of 30 m from the Geospatial Data Cloud (http://www.gscloud.cn/).

The 1:50,000 geological map used to excise non-karst areas in remote sensing images is from the Karst Scientific Data Centre.

The land use type map data for extracting water bodies, construction, and other plots in remote sensing images are obtained by performing band extraction and using the remote sensing images of each year.

DEM data for altitude and slope for geodetic analysis of the main drivers of KRD are derived from Geospatial Data Cloud with average annual precipitation from the Karst Scientific Data Centre and soil erosion data from Southern Karst Desertified professional database (Table 1).

Research ideas

Prediction method of KRD using CA model and geodetector, including the four stages, preprocessing and inputting, subsystem parameter correction and decision-making, and output of land-based change. The research framework is shown in Fig. 2.

The preliminary data preparation stage mainly includes the data of KRD in 2011 and 2016 and the six KRD type occurrences, such as lithology, elevation, slope, annual average precipitation, soil erosion, and resident population density. Factors data are as follows: data preprocessing and input stage, processing of KRD data, and impact factors data to obtain a comprehensive geographic information database with a consistent data structure and geographical coordinates. Subsystem calibration is used in obtaining the parameters of the model system application, which are a matrix of calculation of influence factors based on geodetector, probability of land use transfer probability matrix predicted by Markov model and calculation of each using the multi-criteria evaluation land use driver weight matrix. On the basis of the KRD map, the optimum transition rule is used in determining the types of CULs (Fig. 2).

Selection of driving factors of KRD based on geodetector

KRD is an embodiment of the contradiction between humanity and nature. Therefore, the driving factors for the occurrence and evolution of KRD should include two parts, natural factors and social and human factors.

In this paper, we use a factor detector in the geodetector mechanism analysis method to calculate the influence of each factor and determine the main factors that affect KRD (Fig. 3). Geodetector is mainly based on the spatial distribution of geographical differences, by economic and social or natural factors; exploring its mechanism is an important part of geography. The model is as follows:

$$\mathrm{q} = 1-\frac{1}{NS^2}\sum_{h=1}^{L} N_h S_h^2 \tag{1}$$

where q is the detection index of the influencing factors of KRD. NS_2 is the number of samples in the entire area. L is the number of samples in the entire area. h is the number of secondary areas. NS_2 is the overall variance of the entire area. N_hS_h is the sub-level area variance. Assuming that $q \neq 0$, the model is established and the interval of q is [0, 1]. When $q = 0$, the distribution of KRD indicates a random distribution. The larger q value indicates a greater impact of zoning on KRD.

Table 1 The main data source

Data name	Data sources	Website link
Remote sensing image	Geospatial Data Cloud	http://www.gscloud.cn/
1:5 million geological map	Karst Science Data Center	http://www.karstdata.cn/
DEM data	Geospatial Data Cloud	http://www.gscloud.cn/
Average annual rainfall	Karst Science Data Center	http://www.karstdata.cn/
Soil erosion data	Karst Science Data Center	http://www.karstdata.cn/
Resident population density data	Statistical Yearbook	People's Government

Fig. 2 Technical road map of KRD change based on the cellular automaton model and geodetic detectors

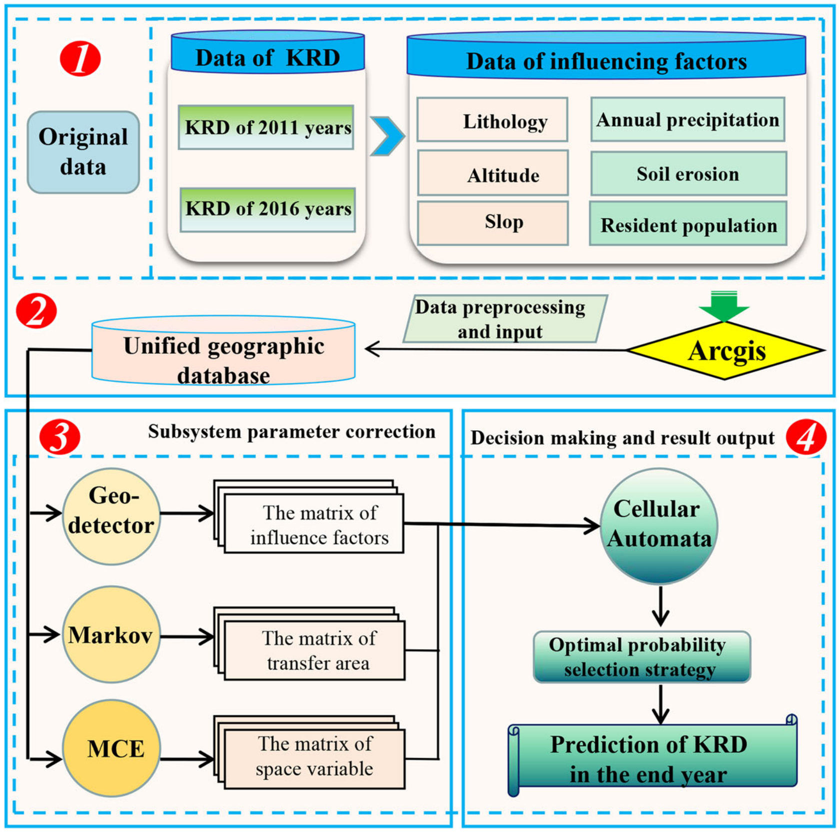

CA–Markov model

Markov forecasting is a means for predicting the probability of an event. The main components of the CA model include cell, state, rules, and neighbors. Each cell is one of a finite number of states, and the states of all the cells are updated at the same time based on the transfer rule. The state of a cell at any one time depends on itself and its neighbors of its previous

Fig. 3 Geographic detector schematic

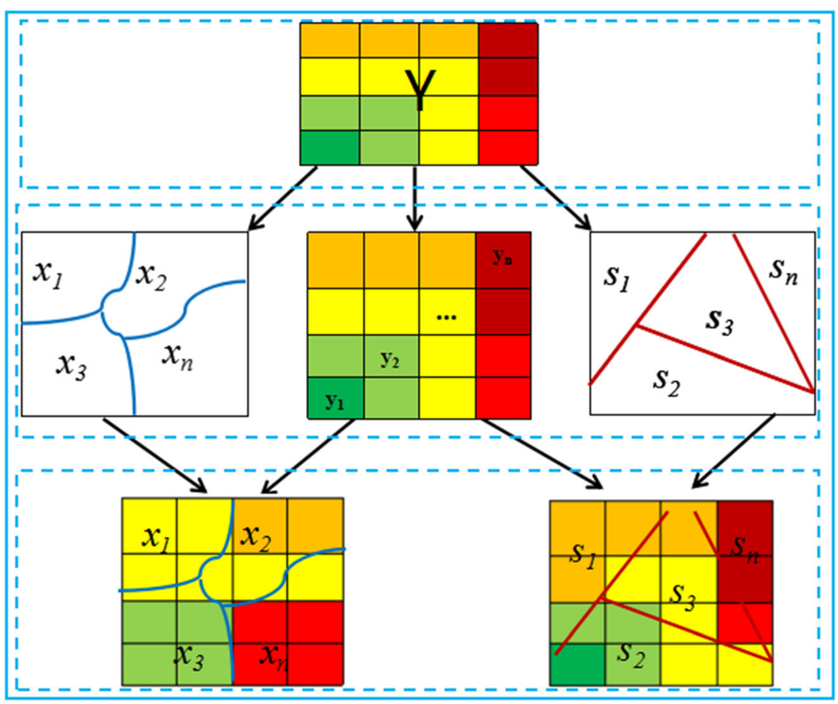

Table 2 Karst rock desertification main driving force of influence

	Lithology	Altitude	Slop	Population density	Average annual precipitation	Soil erosion
q	0.35	0.05	0.21	0.3	0.09	0.16

moment. The use of the CA model can explicitly and directly simulate the evolution of spatial landscape pattern. The CA–Markov model simulates each cell in the spatial distribution pattern of KRD as a single cell, and the type of KRD of each cell is the state of the cell. The logistics module is used to obtain the suitability distribution set and the simulation operation is completed under the CA–Markov module in simulating the change of the spatial pattern of the KRD.

In the research of KRD change, the CA–Markov module process of KRD type and the ratio of the number of transitional areas between KRD types are the state transition probabilities. We predict the change of KRD structure as follows:

$$S(T) = P_{\mathrm{ij}} + S(T_0) \tag{2}$$

In the formula, $S\ (T)$ and $S\ (T_0)$ are the state of KRD at T and T_0, respectively, and P_{ij} is the KRD transition matrix, which can be expressed by Eq. (3):

$$P_{ij} = \begin{bmatrix} P_{11} & P_{12} & \dots & P_{1n} \\ P_{21} & P_{22} & \dots & P_{2n} \\ \dots & \dots & \dots & \dots \\ P_{n1} & P_{n2} & \dots & P_{nn} \end{bmatrix} \tag{3}$$

Results

Driving force factors selection analysis

The occurrence and development of KRD are affected by the combination of natural and social factors. Six influencing factors (altitude, slope, lithology, soil erosion, precipitation, and population density) are selected based on geodetector method (Formula (1)) in identifying the main driving force of the development of KRD. The factor forces calculated by the factor detector in the geodetector survey determine the main factors that affect KRD. The results are as follows: lithology (0.35) > population density (0.30) > slope (0.21) > soil erosion (0.16) > precipitation (0.09) > altitude (0.05) (Table 2).

Overall characteristics of temporal and spatial evolution of KRD

Based on the CA–Markov model, the prediction of KRD change is simulated. Through KRD transition matrix (Table 2) from 2011 to 2016 to establish the conversion rule, the distribution pattern of KRD after 5 years was simulated by the CA–Markov model, and the simulated maps of 2016 and 2021 are obtained (Fig. 4).

Features of KRD in time

Table 3 indicates that the total area of KRD land has changed from 487.12 to 187.57 km^2 from 2011 to 2021, with a net area change of 299.55 km^2 and a reduction rate of 29.955 km^2·a^{-1}. The total area of KRD land is significantly reduced, and the overall KRD land indicates a trend of improvement. At the same time, as can also be seen from Table 3, the area without KRD has increased from 557.19 to 924.54 km^2 in 2011 to 2021 with no significant increase in the area of KRD, thereby indicating other types of KRD. The transfer to non-Karst rock desertification (NKRD) types also reflects the improvement of KRD (Table 3).

Features of spatial evolution of KRD

The spatial distribution of KRD from 2011 to 2021 is shown in Fig. 5. At the start of the study period (Fig. 5a), the KRD in the entire study area was characterized by moderate KRD (MKRD) and medium stone. The two types of KRD account for the vast majority of the space in space even in some areas in which MKRD and extremely severe KRD (ESKRD) occur. The state has invested considerable funds in the management of KRD since the twenty-first century but need 2–3 years to great improvement effect.

The actual interpretation of the distribution of KRD in 2016 (Fig. 5b) indicates that the serious situation of KRD has been greatly improved. The entire study area is dominated by no KRD (NKRD) and potential KRD (PKRD). In the central part of the study area where the trough is flat, minimal distribution of MKRD occurs, and seeing the existence of the types of KRD above severe KRD (SKRD) is difficult. KRD greatly improved from 2011 to 2016.

Based on the distribution of simulative KRD in 2016 by the CA–Markov model (Fig. 5c), compared with the actual interpretation distribution in 2016 (Fig. 5b), the predicted distribution map is mainly light KRD (LKRD) and MKRD. However, it should be noted that the

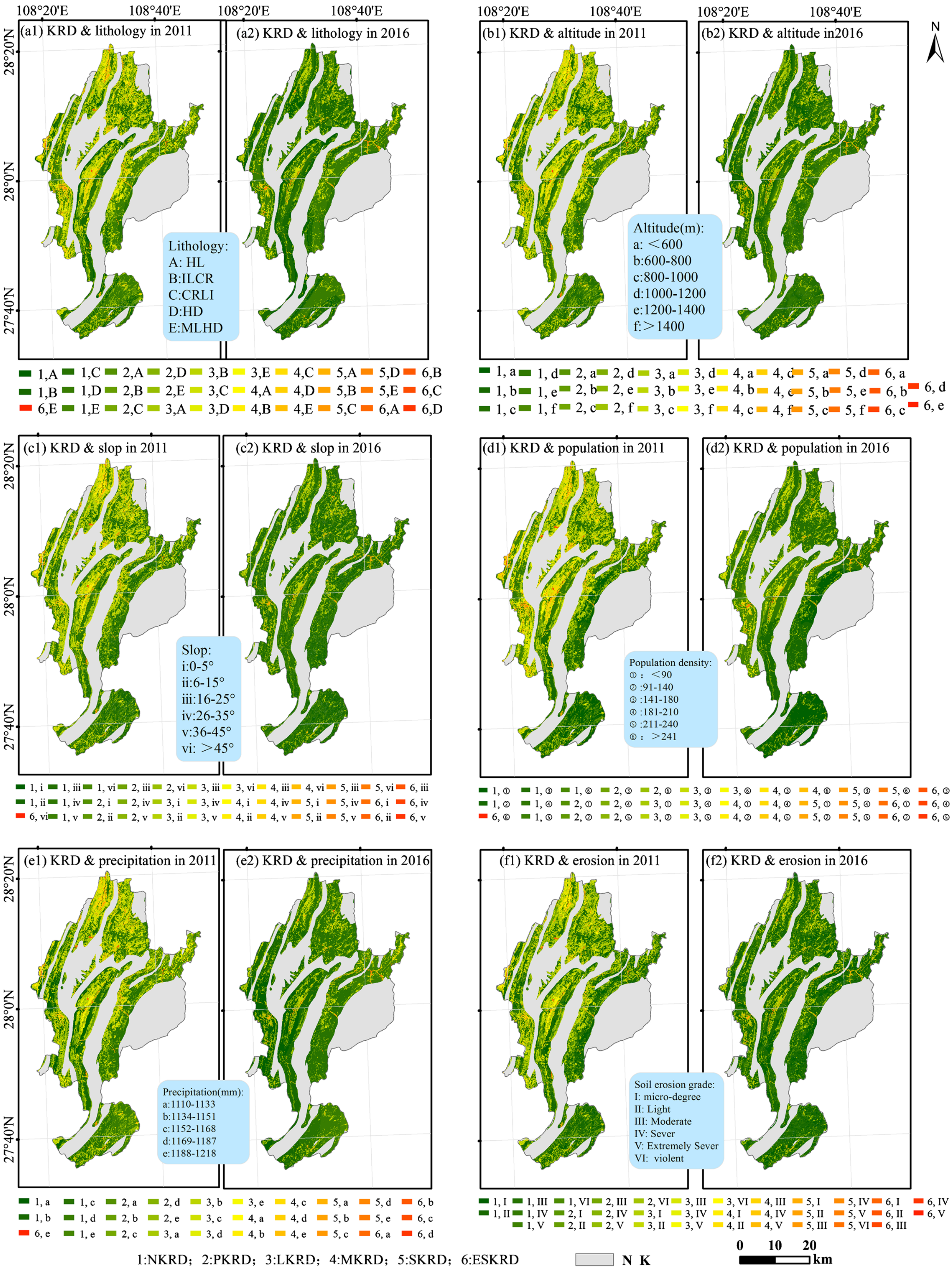

Fig. 4 The influencing factors of KRD. (We make this map by ArcGIS9.3 (http://www.esri.com/arcgis/about-arcgis))

Table 3 Area and ratio of different types of KRD in the study area (2011–2021) (unit: km^2)

Types of KRD land		NKRD	PKRD	LKRD	MKRD	SKRD	ESKRD	KRD
2011	Area **(km^2)**	557.19	132.65	371.63	84.48	21.05	9.96	487.12
	Proportion	47.34	11.26	31.57	7.18	1.79	0.85	41.39
2016	Area **(km^2)**	911.32	62.09	184.79	1.45	16.12	1.99	204.35
	Proportion	77.43	5.28	15.7	0.12	1.37	0.17	17.36
2021	Area **(km^2)**	924.54	61.48	159.55	1.54	24.09	2.39	187.57
	Proportion	78.78	5.24	13.60	0.13	2.05	0.20	15.98

Note: *KRD*, karst rocky desertification; *NKRD*, no KRD; *PKRD*, potential KRD; *LKRD*, light KRD; *MKRD*, moderate KRD; *SKRD*, severe KRD; *ESKRD*, extremely severe KRD

simulation results show that the area of SKRD is increasing compared with 2011. It is because the predicted recovery rate of KRD is slower than the real recovery rate.

Based on the distribution of predictions KRD in 2021 (Fig. 5d), we conclude that in most areas of the study area, mainly MKRD to LKRD, LKRD to PKRD, and PKRD to NKRD gradually improve. Overall, KRD has been effectively improved. At the same time, very few SKRD occur in the eastern part of the study area possibly because people in the valley area have increased their intensity of farming, thereby resulting in an increase in excessive desertification in rare areas.

Dynamic characteristics of the temporal and spatial evolution of KRD

From 2011 to 2016, 540.31 km^2 of land with unchanged KRD area and 10.80 km^2 of LKRD to NKRD accounted for 64.17% of the same change area (Table 4). LKRD to PKRD was 8.41 km^2, thereby accounting for 72.72% of the same change area. At this stage of the period from 2011 to 2016, the area of KRD declined, the proportion of NKRD increased, and the KRD indicated a turnaround (Fig. 6a).

Table 5 shows the following estimated areas and their corresponding changes from 2016 to 2021: 548.91 km^2, unchanged KRD; 103.51 km^2, changed from PKRD to NKRD; 213.79 km^2, changed from PKRD to NKRD; 14.30 km^2, unchanged PKRD; 34.80 km^2, transition from LKRD to PKRD; 95.08 km^2, unchanged LKRD, and 32.22 km^2, changed from MKRD to LKRD. It is not difficult to see from the area of the above transfer changes that from 2016 to 2021, the KRD is improving strongly, showing a shift from the more serious type to the lighter type (Fig. 6b).

The evolution of KRD, the area of specific improvement, or deterioration is unclear in previous studies. On the basis of the intensity change (Fig. 6), we calculated the spatial distribution of the areas with improvement and deterioration (Fig. 7) so as one important reference condition for the following relevant measures.

Figures 7 a and b indicate that in 2011–2016, the area with improved KRD is obviously larger than the deteriorating area. The area with the most obvious improvement is the study area. The northern and central regions also indicate a deteriorating region at this stage, mainly in the areas along the valley. The worsening area increases in 2016–2021 relative to 2011–2016 (Fig. 7d), but the improvement in KRD is also evident in the improved areas (Fig. 7c).

Discussion

Prediction accuracy verification

Change of KRD is an extremely complicated geographical process. Accurately simulating the change of KRD is very difficult due to many factors such as natural conditions, human factors, and social economy (Tian et al. 2017). Therefore, the overall pattern of the change of KRD is even more important. Figs. 5 b and c compare actual KRD and simulated KRD in 2016. The key of model simulation is whether the simulation results are accurate. To solve this key issue, this study uses the following two approaches in model verification.

Pixel-based KRD probability verification

Basing on Fig. 8, we can conclude that the probability distribution of various types of KRD is spatially distributed. The larger the value of a certain area is, the greater the probability of KRD. For instance, in Fig. 8a, the larger the figure in the map is, the greater the probability that the region will develop into NKRD. We combine this figure with the predicted 2016 map of the analysis of the spatial distribution of KRD (Fig. 5c), and we can draw the 2016 NKRD forecast results (Fig. 5c) correctly.

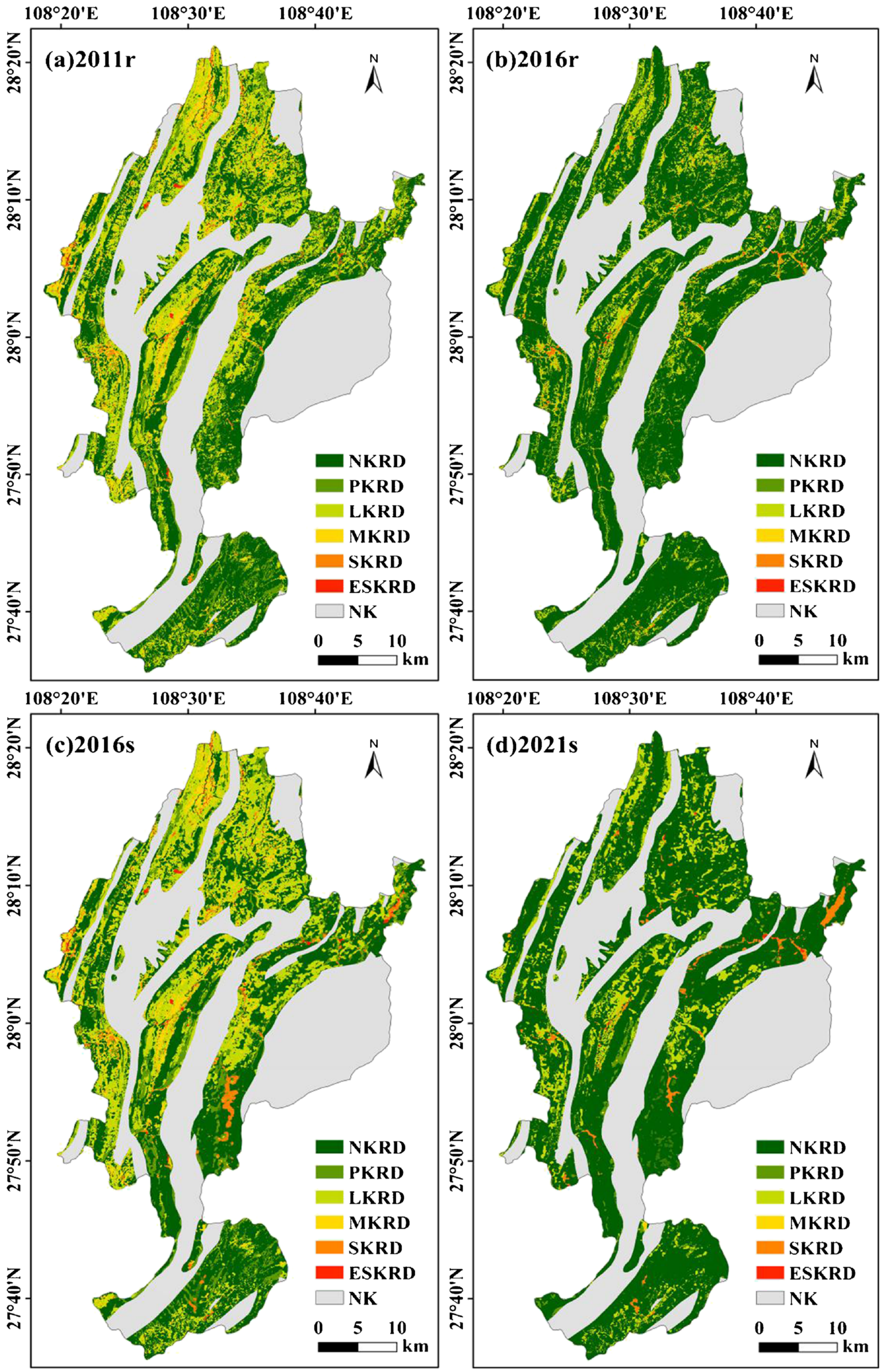

Fig. 5 The distribution of KRD in different periods of the study area. (We make this map by ArcGIS9.3 (http://www.esri.com/arcgis/about-arcgis))

Kappa coefficient test

In order to verify the accuracy of the simulation results quantitatively, kappa coefficient test is carried out on the simulated and the actual interpreted KRD maps. The test results are shown in Table 6. The kappa coefficients are 0.889, 0.541, 0.682, 0.592, 0.766, and 0.504 with NKRD, PKRD, LKRD, MKRD, SKRD, and ESKRD, respectively. These values indicate a certain degree of credibility.

Table 4 KRD intensity rank transfer matrix in the study area (2011–2016) (unit: km^2)

Types	NKRD	PKRD	LKRD	MKRD	SKRD	ESKRD	2011
NKRD	540.31	108.03	219.01	30.75	5.87	6.1	910.07
PKRD	3.85	15.44	38.19	4.12	0.26	0.19	62.05
LKRD	10.8	8.41	109.03	46.47	7.95	1.83	184.49
MKRD	0.12	0.18	0.61	0.41	0.1	0.03	1.45
SKRD	1.89	0.42	3.18	2.42	6.41	1.78	16.1
ESKRD	0.17	0.06	1.05	0.24	0.44	0.03	1.99
2016	557.14	132.54	371.07	84.41	21.03	9.96	1176.15

Table 5 KRD intensity grade transfer matrix in 2016–2021(unit: km^2)

Types	NKRD	PKRD	LKRD	MKRD	SKRD	ESKRD	2021
NKRD	548.91	5.90	15.31	0.54	4.41	0.31	575.38
PKRD	103.51	14.30	10.72	0.13	2.63	0.37	131.66
LKRD	213.79	34.80	95.08	0.30	2.91	1.01	347.89
MKRD	42.36	5.50	32.22	0.51	1.91	0.23	82.73
SKRD	13.32	0.69	4.59	0.03	9.96	0.42	29.01
ESKRD	6.21	0.22	1.52	0.02	2.23	0.03	10.24
2016	928.09	61.42	159.43	1.55	24.06	2.37	1176.15

Temporal and spatial evolution of KRD

Since the start of the twenty-first century, the total area of KRD in the study area has obviously changed, and KRD has indicated a trend of improvement. Analysis of the causes, evolution pattern of KRD is a combination of natural factors and human activities (Li et al. 2017; Li et al. 2018; Chen et al. 2018). During the period of 2011–2021, the main reason for the strong improvement of KRD is that with the continuous development of urbanization, a large number of rural labor force is liberated from the land to other work. The deterioration trend of KRD will be slowed down even began to improve. Meanwhile, the implementation of the ecological environment control project will promote the improvement of KRD, but it has a certain delay (Wu et al. 2017; Zhang et al. 2013). After the implementation of the project, there will be 2 or 3 years to see that the KRD is obviously improved.

Deficiencies and prospects

The change of KRD is a complex system, and cellular automata is an important tool that is suitable for the simulation of complex systems. The model indicates a strong spatial self-organization ability and a great advantage for simulated KRD. In recent years, one aspect of research is mainly focused on the use of artificial intelligence for obtaining the transformation rules in improving the quality of the simulation. However, the artificial intelligence

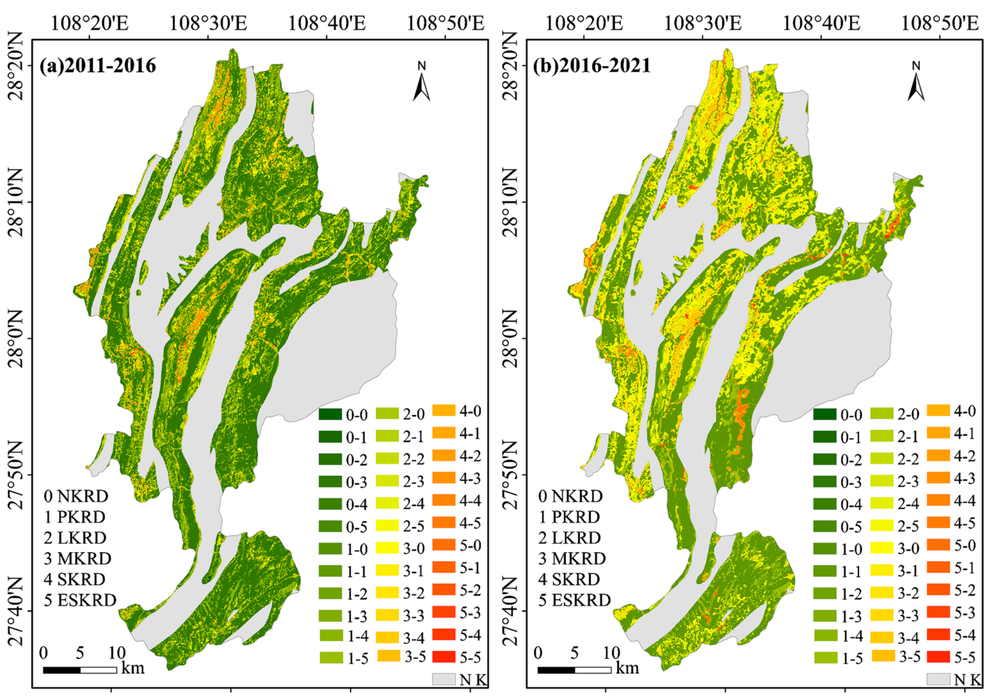

Fig. 6 Change trend of KRD intensity in different periods of the study area

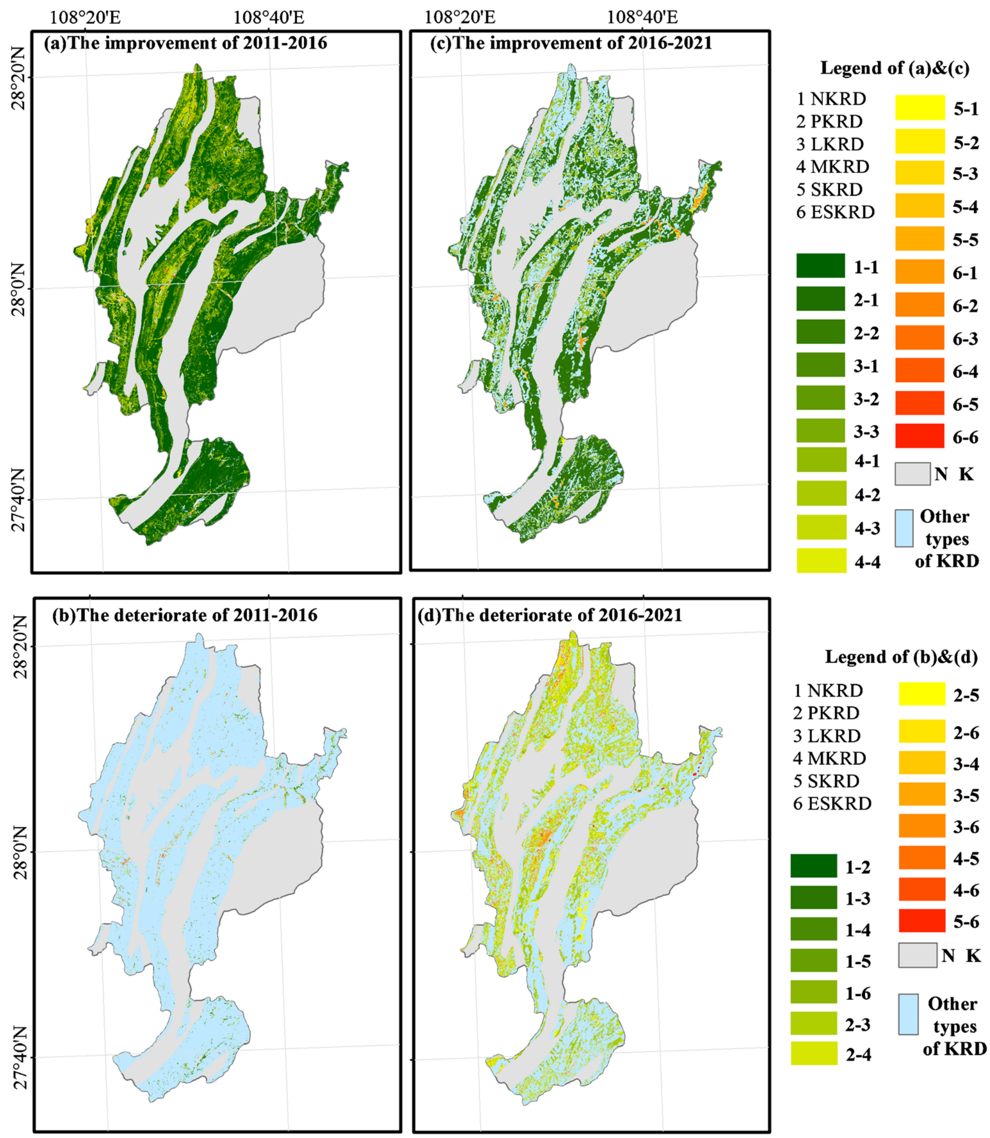

Fig. 7 Spatial distribution map of KRD improvement and deterioration in the study area

method is mostly a black box model, which is not conducive to the discovery of the rules hidden under the change of spatial pattern. By contrast, in all types of cellular automata expansion models that do not use AI, most of them can only simulate one type of target class and simulate and explore many types of land classes. In future research, the improvement of the ability to analyze and simulate models in the comprehensive relationship is essential to ensuring that the simulation results are nearer the real situation of future development.

Conclusion

(1) The CA model is used for the simulation of the spatial distribution of KRD. The kappa coefficient of all types of KRD is over 0.5, thereby meeting the theoretical requirements and accurately representing the future distribution of KRD.

(2) Analysis of KRD driving factors that used the geodetector model can accurately screen the driving factor, factor intensity for lithology (0.35) > population density (0.30) > slope (0.21) > soil erosion (0.16) > the annual precipitation (0.09) > altitude (0.05).

(3) The compound use of geographic detector and CA–Markov model compound use can more accurately predict the future evolution trend of KRD, reduce the subjective factor of randomness, and reduce errors in the prediction of KRD scenarios in the future, thereby ensuring accuracy.

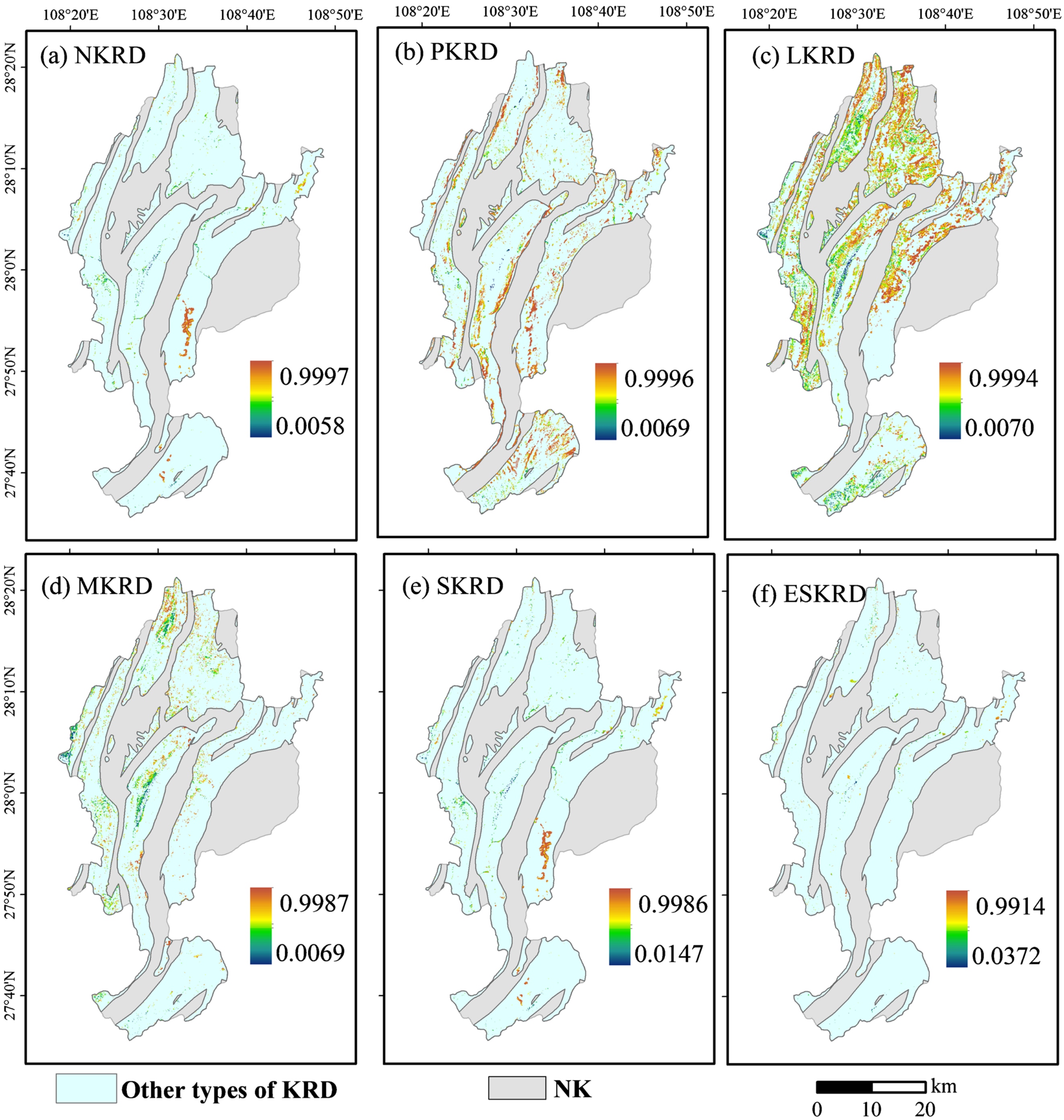

Fig. 8 Spatial distribution of probability of occurrence of various types of KRD in 2016 forecast results

(4) From 2011 to 2021, the total area of KRD in the study area decreased at a rate of 29.96 $km^2 \cdot a^{-1}$, and KRD land indicated an overall trend of improvement. Under the trend of overall improvement of KRD, a few areas remain in which KRD increased and deteriorated. In the process of governance and protection, we focus on the deterioration of the ecological environment.

Table 6 Kappa coefficient test

True interpretation data	Predicted data	Kappa
2016r-NKRD	2016s-NKRD	0.889
2016r-PKRD	2016s-PKRD	0.541
2016r-LKRD	2016s-LKRD	0.682
2016r-MKRD	2016s-MKRD	0.592
2016r-SKRD	2016s-SKRD	0.766
2016r-ESKRD	2016s-ESKRD	0.504

Funding This research work was supported jointly by National Key Research Program of China (Nos. 2016YFC0502102 and 2016YFC0502300), "Western light" talent training plan (Class A), Chinese Academy of Science and Technology services network program (No. KFJ-STS-ZDTP-036) and International Cooperation Agency international partnership program (No. 132852KYSB20170029, No. 2014-3), Guizhou high-level innovative talent training program "ten" level talents program (No. 2016-5648), United Fund of Karst Science Research Center (No. U1612441), international cooperation research projects of the National Natural Science fund committee (Nos. 41571130074 and 41571130042), and Science and Technology Plan of Guizhou Province of China (No. 2017–2966).

Declarations

Competing interests The authors declare no competing interests.

References

Arsanjani JJ, Helbich M, Kainz W et al (2013) Integration of logistic regression, Markov chain and cellular automata models to simulate urban expansion[J]. Int J Appl Earth Obs Geoinf 21: 265-275

Bai XY, Wang SJ, Xiong KN (2013) Assessing spatial-temporal evolution processes of karst rocky desertification land: indications for restoration strategies. Land Degrad Dev 24:47–56

Berjak SG, Hearne JW (2002) An improved cellular automaton model for simulating fire in a spatially heterogeneous Savanna system. Ecol Model 148(2):133–151

Chen F, Zhou DQ, Bai XY et al (2018) Spatial -temporal evolution of Karst Rocky desertification and future trends based on CA-Markov methods in Typical Karst Valley[J]. J Agric Resour Enviro 35(2): 174–180

Geist H (2006) Land-use and land-cover change: Local processes to global impacts. Springer

Han Y, Ko S (2012) Analysis of a cellular automaton model for car traffic with a junction. Theor Comput Sci 450:54–67

Jin X, White R (2012) An agent-based model of the influence of neighbourhood design on daily trip patterns. Comput Environ Urban Syst 36(5):398–411

Lambin EF, Geist H (2006) Global change - the igbp series land-use and land-cover change || searching for the future of land: scenarios from the local to global scale. pp 137–155. https://doi.org/10.1007/3-540-32202-7(Chapter6)

Li Yb, Bai XY, Qin XC et al (2006) The correlation analysis of desertification of karst rock and land use patterns. Resources Sci 28(2):67–73

Li Yb, Bai XY, Wang SJ et al (2017) Evaluating of the spatial heterogeneity of soil loss tolerance and its effects on erosion risk in the carbonate areas of southern China. Solid Earth 8(3):661–s669. https://doi.org/10.5194/se-8-661-2017

Lárraga ME, Alvarez-Icaza L (2010) Cellular automation model for traffic flow based on safe driving policies and human reactions. PHYSICA A 389(23):5425–5438

Li HW, Wang SJ, Bai XY, Luo WJ, Tang H, Cao Y, Wu LH, Chen F (2018) Spatiotemporal distribution and national measurement of the global carbonate carbon sink. Sci Total Environ 643:157–170. https://doi.org/10.1016/j.scitotenv.2018.06.196

Long Y, Han HY, Mao Q (2009) Establishing urban growth boundaries using constrained CA. Acta Geograph Sin 64(8):999–1008

Muci AL, Jorquera MA, Ávila ÁI et al (2012) A combination of cellular automata and agent-based models for simulating the root surface colonization by bacteria. Ecol Model 274:1–10

Neumann JV (1996) Theory of self-reproducing automata. University of Illinois

Perez L, Dragicevic S (2012) Landscape-level simulation of forest insect disturbance: coupling swarm intelligent agents with GIS-based cellular automata model. Ecol Model:53–64

Perry G (1998) Current approaches to modelling the spread of wildland fire: a review. Prog Phys Geogr 22(2):222–245

Qiu BW, Chen CC (2008) Land use change simulation model based on MCDM and CA and its application. Acta Geograph Sin 63(2):165

Quartieri J, Mastorakis NE, Iannone G, Guarnaccia C (2010) A cellular automata model for fire spreading prediction. PHYSICA A:173–178

Rasmussen R, Hamilton G (2012) An approximate Bayesian computation approach for estimating parameters of complex environmental processes in a cellular automata. Environ Model Softw 29(1):1–10

Sun J, Zhang L, Peng C et al (2012) CA-based urban land use prediction model: a case study on orange county, Florida, US. Journal of Transportation Systems Engineering and Information Technology 12(6):85–92

Tian YC, Bai XY, Wang SJ, Qin LY, Li Y (2017) Spatial-temporal changes of vegetation cover in Guizhou Province, Southern China. Chin Geogr Sci 27(1):25–38. https://doi.org/10.1007/s11769-017-0844-3

Wang SJ (2002) History of the concept of karst rocky desertification and its scientific connotation study. China karst 21(2):101–104

Wang Y, Li S (2011) Simulating multiple class urban land-use/cover changes by RBFN-based CA model. Comput Geosci-Uk 37(2):111–121

Wang SJ, Li YB, Li RL (2003) Karst rocky desertification: formation background, evolution and comprehensive taming. Quaternary Sciences 23(6):657–666

Wang SJ, Li RL, Sun CX, Zhang DF, Li FQ, Zhou DQ, Xiong KN, Zhou ZF (2004) How types of carbonate rock assemblages constrain the distribution of karst rocky desertified land in Guizhou Province, PR China. Land Degrad Dev 15:123–131. https://doi.org/10.1002/ldr.591

Wolfram S (1984) Universality and complexity in cellular automata. PHYSICA D 10(1):1–35

Wolfram S (2002) New kind of science. Wol- fram Media.Wolfram, S, Urbana-Champagne, IL

Wu LH, Wang SJ, Bai XY (2017) Quantitative assessment of the impacts of climate change and human activities on runoff change in a typical karst watershed, SW China. Sci Total Environ 601-202(1):1449–1465. https://doi.org/10.1016/j.scitotenv.2017.05.288

Xiong KN et al (2009) Evolutional trend and integrated rehabilitation of karst rocky desertification with a special reference to Guizhou Province. Symposium on ecological construction and regional scientific development of the Yangtze River Basin 18-23

Yang J, Wang Z, Yang D et al (2009) Ecological risk assessment of genetically modified crops based on cellular automata modeling. Biotechnol Adv 27(6):1132–1136

Yang QQ, Wang KL, Zhang CH, Yue YM, Tian RC, Fan FD (2011) Spatio-temporal evolution of rocky desertification and its driving forces in karst areas of Northwestern Guangxi, China. Environ Earth Sci 64:383–393. https://doi.org/10.1007/s12665-010-0861-3

Yassemi S, Dragićević S, Schmidt M (2008) Design and implementation of an integrated GIS-based cellular automata model to characterize forest fire behaviour. Ecol Model 210(1/2):71–84

Yuan DX (2008) Global view on karst rock desertification and integrating control measures and experiences of China. Pratacultural Science 25(9):19–25

Zhang MY et al (2013) Spatial China distribution and change of vegetation carbon in Northwest Guangxi, on the basis of vegetation inventory data. Acta Ecol Sin 33(16):5067–5077. https://doi.org/10.5846/stx6201205170739

Zuo TA, Diao CT, Su WC, Sun XF, Guan DJ (2014) Spatial-temporal evolution process and its evaluation characteristic of rocky desertification in Bijie experimental area. Acta Ecol Sin 34(23):7067–7077. https://doi.org/10.5846/stxb201401140108